Hindawi
Journal of Chemistry
Volume 2017, Article ID 9513438, 9 pages
https://doi.org/10.1155/2017/9513438

Research Article

LIBS Analysis of Geomaterials: Comparative Study of Basalt Plasma Induced by TEA CO_2 and Nd:YAG Laser in Air at Atmospheric Pressure

Jelena Savovic,[1] Milos Momcilovic,[1] Sanja Zivkovic,[1] Andrei Stancalie,[2] Milan Trtica,[1] and Miroslav Kuzmanovic[3]

[1] *Vinča Institute of Nuclear Sciences, University of Belgrade, Mike Alasa 12-14, 11001 Belgrade, Serbia*
[2] *National Institute for Laser, Plasma and Radiation Physics, Center for Advanced Laser Technologies (CETAL), Atomistilor 409, 077125 Magurele, Romania*
[3] *Faculty of Physical Chemistry, University of Belgrade, Studentski trg 12-16, 11000 Belgrade, Serbia*

Correspondence should be addressed to Jelena Savovic; lelas@vin.bg.ac.rs

Received 30 March 2017; Revised 30 May 2017; Accepted 7 June 2017; Published 11 July 2017

Academic Editor: J. O. Caceres

We present a study of the plasma generated by transversely excited atmospheric (TEA) CO_2 laser irradiation of a basalt sample. The plasma was induced in air at atmospheric pressure. The same sample was also analyzed using a commercial LIBS system based on Nd:YAG laser and time-gated detection. The main plasma parameters, temperature, and electron number density were determined and analytical capabilities of the two systems compared. Despite differences in laser wavelength, pulse duration, applied fluence, and signal detection scheme, the two systems are comparable in terms of element detectability and limits of detection. In both cases, all elements usually present in geological samples were identified. The estimated limits of detection for most elements were below 100 ppm, while for Cu, Cr, and Sr they were around or below 10 ppm. The obtained results led to the conclusion that simple, cost-effective TEA CO_2 LIBS system can find applications for geological explorations.

1. Introduction

The data on the chemical composition of geomaterials are of fundamental importance for exploitation and use of georesources, environmental studies, and space explorations. Because of that, development of rapid and accurate instrumental analytical methods for chemical analysis of geological materials is of prime importance. At the same time, the analysis of geomaterials is often a challenging analytical task, as it requires determination of a large number of elements, over a wide range of concentrations, in a variety of complex matrices.

The well-established spectrochemical techniques that are mainly used in this field are inductively coupled plasma optical emission spectroscopy (ICP-OES), inductively coupled plasma mass spectrometry (ICP-MS), and X-ray fluorescence (XRF) spectroscopy. In recent years, a considerable progress has been made in the development of another spectrochemical technique, laser-induced breakdown spectroscopy (LIBS) [1]. LIBS combines capability of providing fast multielemental analysis with no sample pretreatment, potential for in situ and remote analysis, the ability to perform surface and depth profiling, and the ability to provide isotopic ratio information additionally to elemental composition [2]. Regarding the analysis of geomaterials, LIBS has certain advantages compared to ICP and XRF. ICP-OES and ICP-MS have better analytical figures of merit such as accuracy and precision and limits of detection compared to LIBS. However, many geological samples are silicate rocks, and the main benefit of LIBS compared to ICP is that there is no need for solid sample digestion, that is, no need for complex and time-consuming dissolution procedures. On the other hand, XRF spectrometry is a rapid method for in-field elemental analysis of geological samples and requires simple and minimal

sample preparation (e.g., fusion or preparation of pressed pellets) [3]. These characteristics are also common to LIBS. At the same time, compared to XRF, LIBS has higher sensitivity for elements like Mg, Si, Al, Ca, and K and especially for light elements like Li, Be, B, C, F, and Na. Also, unlike ICP and XRF, LIBS may be easily applied for depth profiling by repeated ablation of the same location. In summary, each of the aforementioned analytical techniques is characterized by its own strengths and weaknesses, and the choice of the "best" technique is dictated by the analytical problem that has to be solved. In that sense, LIBS may be considered as spectrochemical technique complemental to ICP and XRF.

Due to its unique characteristics, LIBS can be used for elemental analysis of almost any type of material. However, the vast majority of LIBS applications deal with compact solid samples and, among them, perhaps the most analyzed sample types were geological materials. LIBS has been successfully applied, both in laboratory setting and in the field, for chemical analysis of rocks, soils, sediments, and other natural materials [2, 5–10]. One of the main problems in quantitative LIBS analysis of complex matrices (such as geological samples) comes from the matrix effects which can reduce the accuracy and precision of the analysis [1, 2, 11]. A number of calibration strategies were proposed for compensation of matrix effects in LIBS, for example, different normalization procedures as well as calibration-free approach [2, 9].

In this work, a recently developed LIBS system, based on transversely excited atmospheric (TEA) CO_2 laser and time-integrated signal detection [12], was applied to the qualitative analysis of basalt samples in air at atmospheric pressure. The basaltic rock was chosen as a representative of geological samples. Basalt is a very important rock as it is the most common rock in Earth's crust and is also an abundant rock on other satellites and planets, for example, Moon and Mars [13]. TEA CO_2 laser-based LIBS has been previously applied for the analysis of basalt under simulated Martian atmospheric conditions (CO_2 gas; pressure: 9 mbar) [4]. It was shown that this LIBS system provides good analytical capabilities for geological studies under low-pressure CO_2 gas. Although LIBS under different atmospheric conditions offers the possibility to improve the resolution, signal intensity, and signal-to-noise ratio or enable specific applications, it also introduces a degree of complexity in the experimental setup. Thus, the present study was undertaken to examine the possibility of using TEA CO_2 laser-based LIBS for the analysis of geologic samples in air at atmospheric pressure. The same sample was also analyzed using a commercial LIBS system based on Nd:YAG laser and time-gated detection.

Currently, the most common LIBS system used for the analysis of geological samples comprises Nd:YAG laser and time-gated detection [5–10]. Compared to it, the main advantage of TEA CO_2 laser-based LIBS is simplification of the instrumentation. The characteristics of TEA CO_2 laser (wavelength and pulse duration) make this laser especially suitable for time-integrated measurements, which precludes the use of delay generators and expensive gated detectors required for time-resolved measurements. Differences in laser wavelength and pulse duration for the two laser sources (10.6 μm, 100 ns for TEA CO_2 compared to 1.064 nm, 7 ns for Nd:YAG) inevitably influence the ablation process, the plasma parameters, and plasma expansion dynamics. Excitation wavelength has a strong influence on the laser-target and laser-plasma interactions. Mass ablation rate per pulse (m) is higher for shorter wavelengths ($m \sim \lambda^{-4/9}$) [14]. However, when operating with infrared wavelengths, dominant mechanism for laser-plasma interaction is *Inverse Bremsstrahlung* (IB) absorption. The rate of IB absorption (αIB) increases as the laser wavelength increases ($\alpha\text{IB} \sim \lambda^3$) [14]. Thus, for Nd:YAG plasma, a higher ablation efficiency may be expected, while laser-plasma interaction is expected to be much stronger in the case of CO_2 laser. Efficient IB absorption reheats the plasma, causing an additional plasma excitation and expansion. In LIBS, only a fraction of the analyte mass is excited and is capable of producing detectable optical emission. Higher excitation efficiency in CO_2 plasma may compensate the lower ablation efficiency. In addition, the dimensions and lifetime of plasma increase with pulse duration. The plasma takes longer to decay and, hence, the emission lasts longer. With the long-pulse irradiation, the excitation of the plasma is rather gradual, and, hence, it is suitable to obtain highly excited plasma.

The analytical capabilities of the two LIBS systems were compared in terms of detectability and limits of detection (LODs). A simplified single-sample method was applied for estimation of LOD [15]. Elemental composition of the basalt sample was determined by ICP analysis. Also, plasma parameters, temperature, and electron number density for plasma created by CO_2 and Nd:YAG laser pulses were evaluated and compared.

2. Experimental

2.1. The Sample. The rock sample used in the present work was the same as the one used in our previous study [4], that is, a Tertiary basaltic rock from the Balkan Peninsula, classified according to the TAS scheme as basaltic trachyandesite [16]. A sample was prepared by cutting the original natural basaltic rock to a piece about 35 mm long and ~5 mm thick. The sample was used as is, without any preparation. Elemental composition of the sample was determined by ICP analysis. Samples for ICP analysis were prepared by alkaline fusion procedure [17]. For the major elements, 40 mg of powdered material was fused with LiBO flux and then dissolved in dilute HNO_3. For the trace elements, $HF/HClO_4/HNO_3$ dissolution was undertaken using 100 mg of sample. Five analyses were completed to determine measurement precision. Elemental composition of the sample is given in Table 1.

2.2. TEA CO_2 LIBS System. The experimental setup is described in prior publication [4, 18] and is briefly summarized here. A commercial TEA CO_2 laser system, developed at Vinča Institute, was used as the energy source for plasma generation on the basalt samples [19]. Pulsed TEA CO_2 laser emits radiation at 10.6 μm, with an output peak power typically in the order of megawatts. The laser-optical pulse has a gain-switched spike, followed by a slowly decaying tail. The full width at half maximum (FWHM) of the spike

Table 1: Elemental composition of basaltic rock obtained using ICP-OES analysis [4].

Concentration* (wt%)									
SiO_2	TiO_2	Al_2O_3	Fe_2O_3	MnO	MgO	CaO	Na_2O	K_2O	P_2O_5
53	1.1	12.2	5.7	0.10	4.8	4.8	2.4	5.7	1.2
Concentration (μg/g)									
Cr	Ni	Co	V	Cu	Zn	Ba	Sr	Zr	B
300	100	60	120	70	130	2000	740	160	127

*The relative expanded standard uncertainty ranged from 1–3%, in 100 ppm concentration range, to 7–15% for the highest measured concentrations.

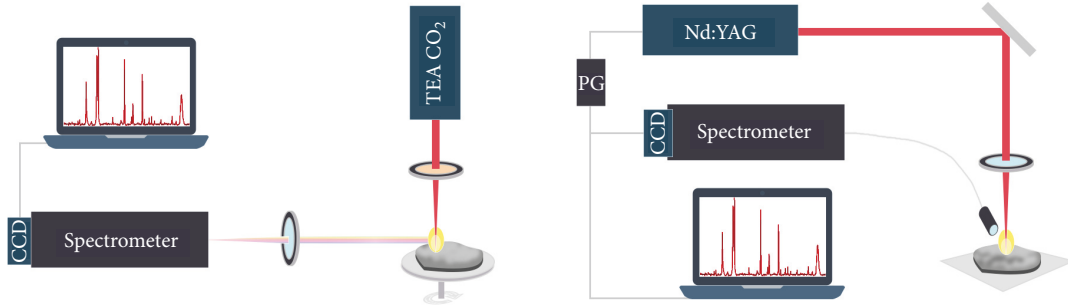

Figure 1: Schematic diagram of the experimental setup used for LIBS analysis. (a) TEA CO_2 laser, nongated signal detection; (b) Nd:YAG laser, gated signal detection.

is about 100 ns, and the tail is about 2 μs. About 35% of the total irradiated laser energy is consisted in the initial spike. Typical output pulse energy was 160 mJ. The sample surface was irradiated by laser light focused using a ZnSe lens (focal length: 130 mm). The angle of incidence of the laser beam with respect to the surface was 90°. The sample was mounted on a rotating sample holder. Single-shot craters well separated in space were achieved by rotation of the sample, while repeated ablation of the same circular path was avoided by lateral movement of the sample.

The optical emission from the plasma was viewed in the direction parallel to the target surface (Figure 1(a)). A time-integrated space-resolved laser-induced plasma spectroscopy (TISR-LIPS) was applied [12, 20–23]. Spatial resolution was achieved by changing the position of the plasma along the direction of the incoming laser beam. The focusing lens and the target holder were placed on positioning stages (three-axis translation stage; travel: 25 mm; resolution: 10 μm) to maintain focus during experiments. For spatially resolved measurements, it was essential to find plasma region, where spectral continuum background intensity is low, while the discrete line signal intensity is high. The optimization was performed by monitoring the signal-to-background ratio (SBR) of several elements (Mg: 285.2 nm, Ca: 393.4 nm, Mn: 403.08 nm, and Fe: 358.12 nm lines) as a function of the viewing position. Different spatial regions of the plasma were sequentially examined by moving the target holder in steps of 100 μm. Highest SBR values were obtained at distances 2 mm away from the sample surface. Thus, in all reported experiments, the observing position was set to 2 mm from the target surface. The horizontal part of the plume was projected by an achromatic lens on the entrance slit of the monochromator (entrance slit width: 30 μm; height: 1 mm; magnification: 1 : 1). The monochromator was equipped with diffraction grating with 600 lines/mm (dispersion: 0.7 nm/mm; blaze at 330 nm in the first order). For the time-integrated measurements, Apogee Alta F1007 CCD camera was used. The CCD consists of 1024 × 122 pixels, each of 12 × 12 microns. The total active area is 12.3 × 1.46 mm.

The laser was operated at 1.3 Hz repetition rate, while the shutter of the nongated CCD detector was opened for 30 s. Measurement time was much longer than plasma lifetime; however, the main contribution to the time-integrated spectrum comes from a very limited temporal window. Averaging of many acquired spectra was a procedure used to attenuate the variation of spectral emission, that is, to compensate pulse-to-pulse variations. Each recorded LIBS spectrum is an average spectrum, obtained by accumulation of consecutive spectra from 40 different locations on the sample. This procedure was as a rule repeated in triplicate, and the resulting spectra were averaged. Thus, all reported spectra correspond to an average of 120 laser pulses. A relative standard deviation of measured LIBS signal intensity was 10–15%.

2.3. Nd:YAG LIBS System. Basalt sample was also analyzed by using commercial LIBS system based on pulsed Nd:YAG laser and time-gated detection (Figure 1(b)). This was a LIBSCAN-100 system which was purchased from Applied Photonics Ltd. (UK). As laser source, it is equipped with a Q-switched Nd:YAG laser emitting at 1064 nm (model Quantel Big Sky CFR Ultra GRM), pulse duration of 7 ns, frequency of 10 Hz, and energy up to 100 mJ. The system possesses 8

Table 2: Spectroscopic constants of the Fe II lines (Figure 3) used in Boltzmann plot temperature determination.

Line number	Transition	Wavelength (nm)	$g_k A_{ki}\,(s^{-1})$	E_k (eV)	Acc
1	$3d^6(^5\mathrm{D})4s$ - $3d^6(^5\mathrm{D})4p$	256.253	$1.07E+09$	5.8232247	C+
2		256.347	$6.04E+08$	5.8755874	B+
4		258.258	$3.50E+08$	5.8755874	B+
5		258.587	$7.15E+08$	4.79323573	B+
7		259.154	$3.40E+08$	5.8232247	C+
9		261.382	$4.24E+08$	4.84893717	B+
10		261.762	$2.93E+08$	4.81789816	B
11		262.829	$3.50E+08$	4.83702227	B
3	$3d^6(^3\mathrm{P2})4s$ - $3d^6(^3\mathrm{P2})4p$	257.436	$9.60E+08$	7.3973237	C+
6	$3d^6(^1\mathrm{G2})4s$ - $3d^6(^1\mathrm{G2})4p$	258.795	$1.69E+09$	8.9430267	B+
8	$3d^6(^1\mathrm{I})4s$ - $3d^6(^1\mathrm{I})4p$	259.278	$4.38E+09$	8.8565247	B+

spectrometer channels covering 182–1057 nm spectral range. The acquisition is made on an integration time of 1.1 ms (the smallest) with 1.27 μs delay time from the laser pulse. The signals were averaged on 50 laser pulses. The statistical variability in the LIBS signal was approximately 10%.

A diameter of a focused laser spot was ~1 mm for TEA CO_2 laser and ~1.4 mm for Nd:YAG laser, that is, in both cases well above the grain sizes of the rock sample (<1 mm) [4]. Thus, the influence of grain size on accuracy and precision of the LIBS analyses was not expected to be large [24]. The main contribution to uncertainty comes from fluctuations due to laser energy and high degree of surface roughness.

3. Results and Discussion

LIBS spectra of basalt were recorded in air at atmospheric pressure. All reported spectra are spectra averaged over many laser shots, and the measurements were taken at a number of locations on the sample surface (a fresh surface was exposed to each incident laser pulse) to avoid the problem with sample heterogeneity. Spectra obtained on the basaltic rock sample with a single TEA CO_2 laser pulse using a nongated detection, covering the spectral region from 250 to 520 nm, are shown in Figure 2. The spectra were taken 2 mm from the target surface. For comparison, spectra obtained using LIBS system equipped with pulsed Nd:YAG laser and time-gated detection are also shown. Most of the elements present in the sample were identified (Table 1), including those present in concentrations around or below 100 ppm, like Co, Cr, Ni, and V. As it may be seen from Figure 2, there is no difference with regard to element detectability for the two LIBS systems used, despite the fact that the applied laser intensities differ by one order of magnitude (56 MW/cm^2 and 460/740 MW/cm^2 for TEA CO_2 laser and Nd:YAG laser, resp.). Thus, it may be concluded that excitation conditions in CO_2 plasma are suitable for detection of all elements usually present in geological samples.

The dissociation, ionization, and excitation processes taking place in plasma are related to characteristic parameters of plasma such as temperatures (T) and electron number densities (n_e). Thus, it was of interest to determine these parameters for plasma created by CO_2 and Nd:YAG laser pulses. The excitation temperature was evaluated by Boltzmann's plot method [25] using the equation

$$\ln\left[\frac{\lambda_{ki} I_{ki}}{g_k A_{ki}}\right] = \ln\left[\frac{hcN}{4\pi Z(T)}\right] - \frac{E_k}{k_B T}, \quad (1)$$

where λ_{ki} is the wavelength of the emitted light, I_{ki} is the integrated line intensity of the transition involving an upper level (k) and a lower level (i), g_k is statistical weight of upper level, A_{ki} is the transition probability, h is Planck's constant, c is the velocity of light in vacuum, N is the total number density, $Z(T)$ is the partition function, E_k is excitation energy, and k_B is the Boltzmann constant. For the determination of excitation temperature of the plasma, eleven iron ionic (Fe II) lines were selected as shown in Figure 3. Considering a relatively narrow spectral interval used, the chromatic sensitivity was not taken into account.

The line identifications and different spectroscopic parameters such as wavelength, transition strength ($g_k A_{ki}$), energy E_k, and accuracy of transition probability (B+ ≤ 7%; B ≤ 10%; C+ ≤ 18%) are listed in Table 2 based on reference data [26]. In case of TEA CO_2 LIBS, the whole set of spectral lines listed in Table 2 was used to obtain Boltzmann's plot, whereas in case of Nd:YAG LIBS, lines numbers 3 and 8 were excluded as they were not resolved.

The estimated temperature of CO_2 laser-induced plasma was 14300 K, while that of Nd:YAG plasma was 19900 K and 21900 K for 50 mJ and 80 mJ pulses, respectively (Figure 4).

For both LIBS systems, under applied experimental conditions, high temperature plasma was created. Higher temperatures were obtained in Nd:YAG laser-induced plasma. However, it should be noted that estimated plasma temperatures are not directly comparable, because time-integrated measurements for CO_2 laser plasma provide average values for the spatially selected plasma zone, while for the Nd:YAG LIBS the values correspond to a specific time window.

The electron number density was determined from the measured *Stark* width of Al I 396.15 nm line (Figure 5).

Deconvolution of Stark width from the experimental profile was done by applying the following formula [27, 28]:

$$w_m = w_V = 0.5346 * w_L + \left(0.2169 * w_L^2 + w_G^2\right)^{1/2}, \quad (2)$$

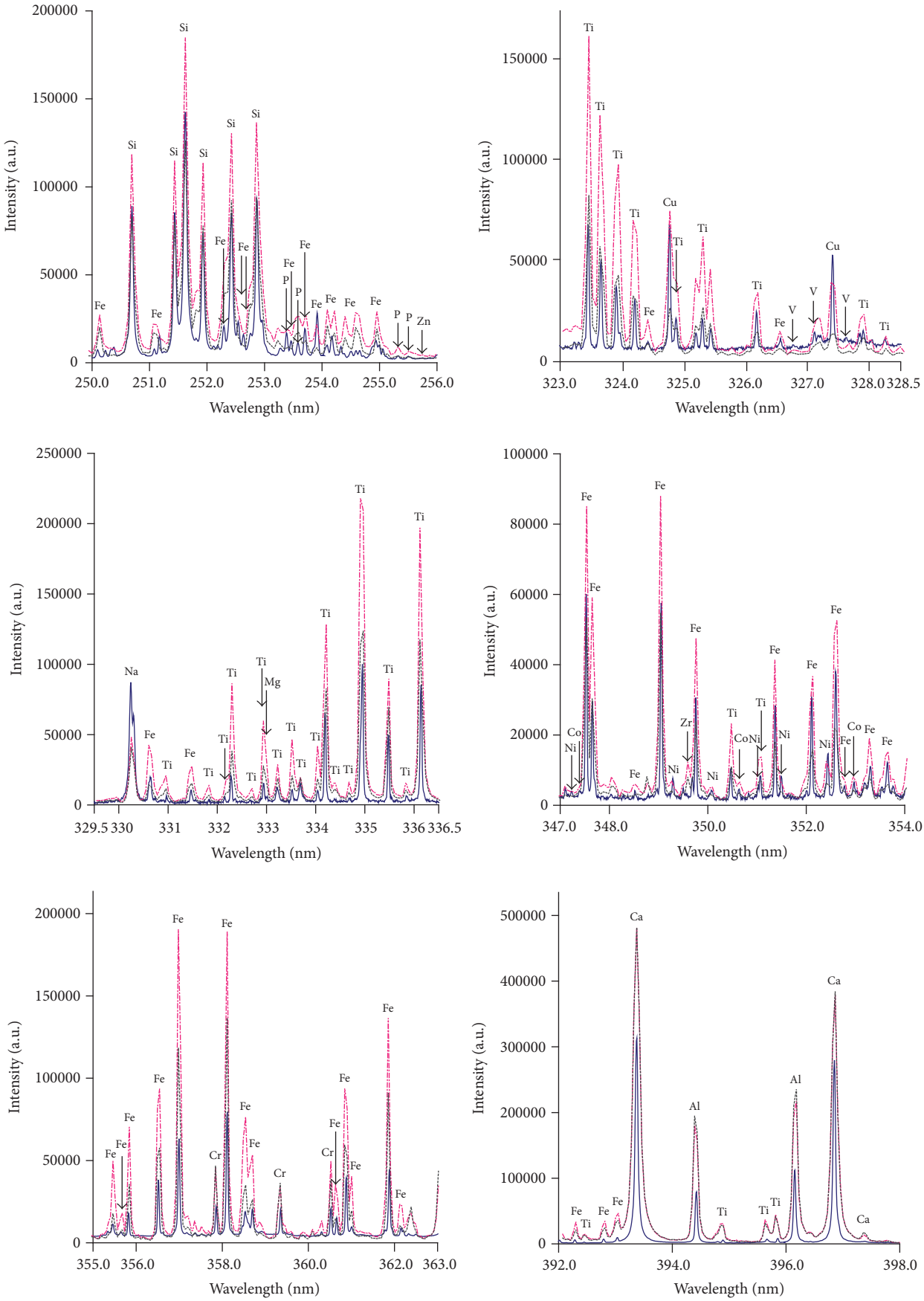

Figure 2: Continued.

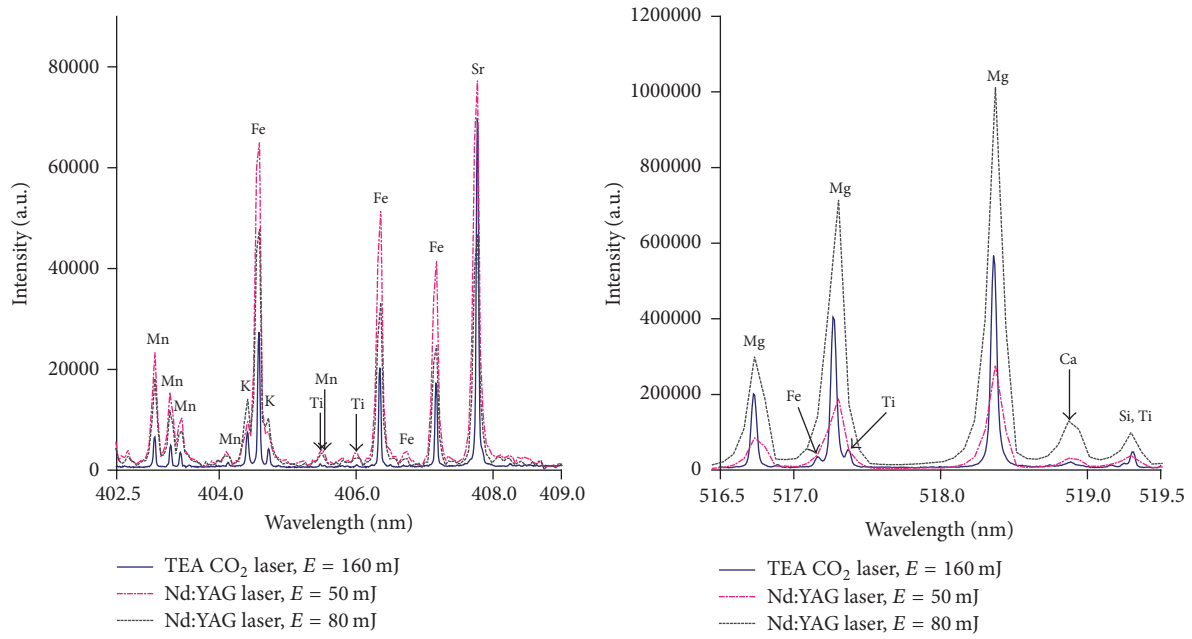

Figure 2: LIBS spectra obtained on the basalt sample with a single TEA CO_2 laser pulse using a nongated detection and with Nd:YAG laser and time-gated detection (delay: 1.27 μs; integration time gate: 1.1 ms). In both cases, the plasma was induced in air at atmospheric pressure.

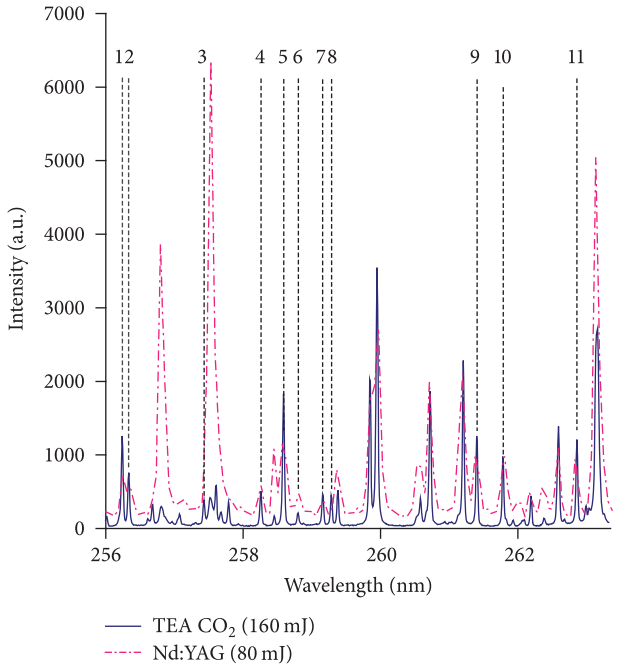

Figure 3: Fe II spectral lines (listed in Table 1) used for calculation of plasma temperature.

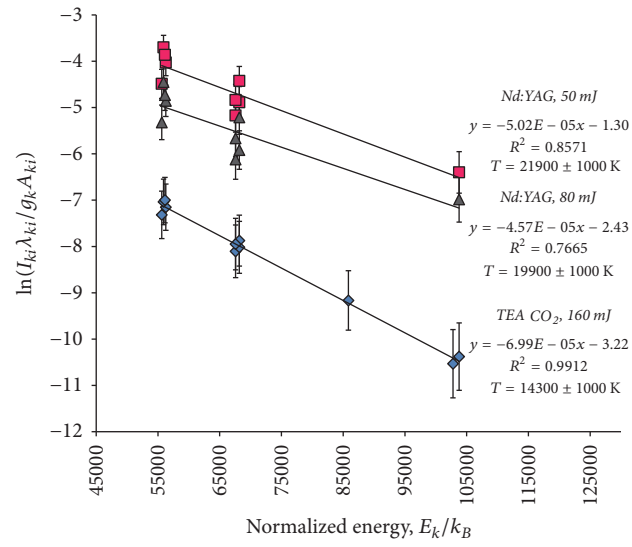

Figure 4: Boltzmann's plot for laser-induced plasma of basalt at atmospheric pressure utilizing Fe II transition lines listed in Table 1. T_{exc} = −1/Slope. The error bars account for combined uncertainties of line intensity measurements and of transition probability accuracy (Table 2).

where $w_L = w_S$, $w_G = (w_D^2 + w_i^2)^{0.5} \approx w_i$, and w_m, w_V, w_L, w_S, w_G, w_i, and w_D are measured, Voigt, Lorentzian, Stark, Gaussian, instrumental, and Doppler width, respectively. For TEA CO_2 LIBS, the instrumental width was measured to be FWHM = 0.025 nm, and, for Nd:YAG LIBS, FWHM = 0.04 nm. An approximate formula was used to determine n_e from deconvoluted Stark widths with Stark broadening parameter taken from [29]:

$$n_e \left[\mathrm{cm}^{-3}\right] = \frac{10^{16}\Delta\lambda_{\mathrm{Stark}}\ [\mathrm{nm}]}{2\omega\ [\mathrm{nm}]}. \quad (3)$$

The obtained values are shown in Table 3.

As seen from Table 3, the estimated electron number densities for the two laser systems are similar. However,

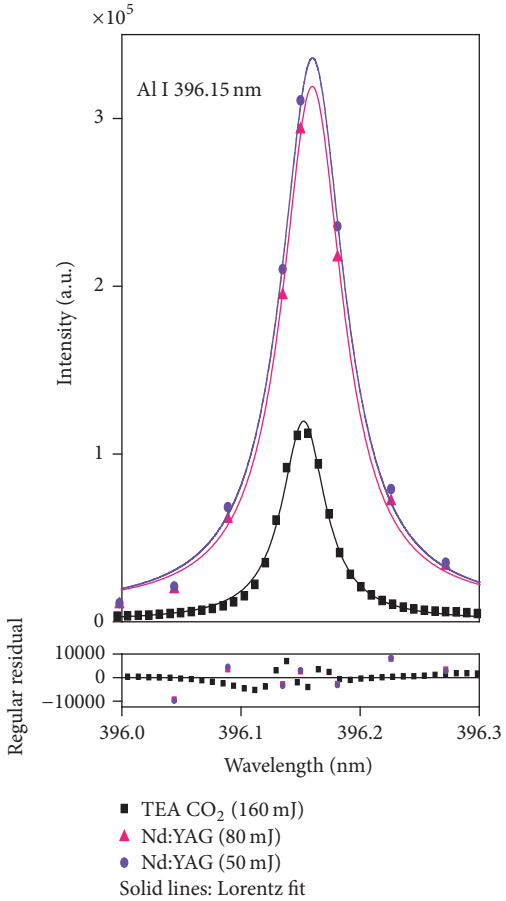

Figure 5: Al 396.15 nm line whose Stark width was used for evaluation of electron number density.

Table 3: Electron number density calculated from Stark width of Al I 396.15 nm line.

LIBS system	w_s, nm	n_e, 10^{16} cm^{-3}
TEA CO_2 laser (160 mJ)	0.033	4.3
Nd:YAG laser (50 mJ)	0.035	4.6
Nd:YAG laser (80 mJ)	0.040	5.3

these values are not directly comparable, as already discussed for the temperature evaluation. Nevertheless, they provide indication of the excitation conditions in plasma.

For both laser systems, spectral data were processed by calculating the integrated peak area of the emission line, the baseline continuum emission intensity, and the root mean square (RMS) noise of the continuum radiation intensity in regions adjacent to the emission line. The signal-to-noise ratio (SNR) was calculated as the integrated peak area A, divided by the width of the peak area w, times the absolute value of the RMS noise: SNR = $A/(w \times \text{rms})$ [30]. Signal-to-noise (SNR) ratio for the elements under study, obtained for TEA CO_2 and Nd:YAG laser-induced basalt plasma, is shown in Table 4.

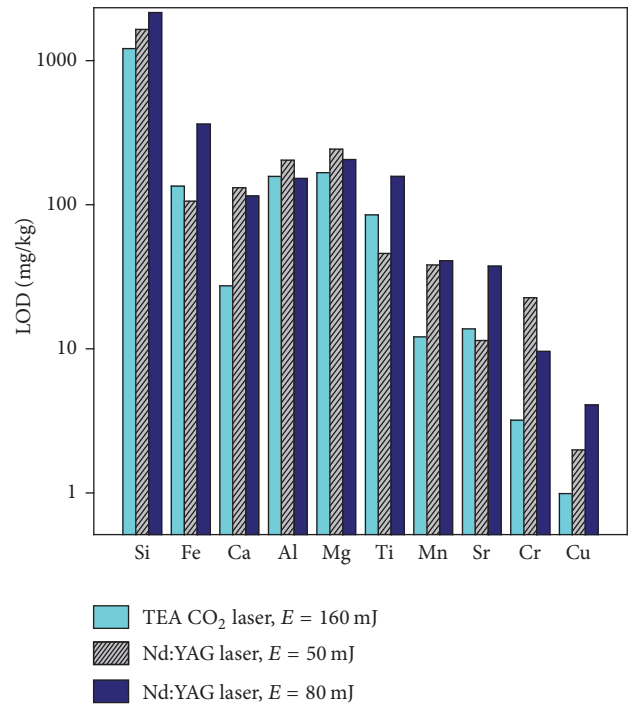

Figure 6: Comparison of estimated limits of detection obtained for TEA CO_2 and Nd:YAG laser-induced plasma over basalt sample in air at atmospheric pressure.

A simplified single-sample method was applied for estimation of the limit of detection (LOD) [15]. LOD was calculated using the formula LOD = $(3 \times c)$/SNR, where c is a known analyte concentration obtained by ICP measurements (Table 1). Comparison of estimated limits of detection obtained for the two laser systems is shown in Figure 6. As it can be seen, comparable or even better LODs were obtained for TEA CO_2 LIBS system. Also, there is no obvious correlation between the energy of the Nd:YAG laser pulse and the estimated LODs.

4. Conclusions

Laser-induced breakdown spectroscopy is based on TEA CO_2 laser and has been applied to elemental analysis of basalt sample. The analysis was done in air at atmospheric pressure without any sample treatment. Results of qualitative analysis were compared to those obtained using a commercial LIBS system based on pulsed Nd:YAG laser. It may be concluded that, with regard to detectability and limits of detection, less complex and cost-effective TEA CO_2 LIBS system has comparable characteristics to the system based on Nd:YAG laser and time-gated detection.

Conflicts of Interest

The authors declare that there are no conflicts of interest regarding the publication of this paper.

Table 4: Comparison of signal-to-noise (SNR) ratio for the elements under study, obtained for TEA CO_2 and Nd:YAG laser induced plasma over basalt sample in air at atmospheric pressure.

Element/line (nm)	Conc.*	SNR		
		TEA CO_2 (160 mJ)	Nd:YAG (50 mJ)	Nd:YAG (80 mJ)
Si I 288.16	24.8%	814	526	454
Fe I 358.12	4.0%	918	342	160
Ca II 393.37	3.4%	3860	913	798
Al I 396.15	6.5%	587	456	611
Mg I 285.21	2.9%	536	368	433
Ti II 334.94	0.66%	236	437	127
Mn I 403.08	774 ppm	199	63	59
Sr II 407.77	740 ppm	165	200	61
Cr I 359.35	300 ppm	293	41	97
Cu I 324.75	70 ppm	218	109	53

*Elemental composition of basalt sample obtained by ICP-OES analysis.

Acknowledgments

This research was supported by (i) the Ministry of Education, Science and Technological Development of the Republic of Serbia through the project "Effects of Laser Radiation on Novel Materials in Their Synthesis, Modifications, and Analysis" (Project no. 172019) and (ii) COST- MP1208 action ("Developing the Physics and the Scientific Community for Inertial Confinement Fusion at the Time of NIF Ignition"). Andrei Stancalie acknowledges financial support of MCI through NUCLEU Programme (ctr. no. PN 1647/2016) and UEFISCDI (ctr. no. 8PM/2010).

References

[1] D. W. Hahn and N. Omenetto, "Laser-induced breakdown spectroscopy (LIBS)—II: review of instrumental and methodological approaches to material analysis and applications to different fields," *Applied Spectroscopy*, vol. 66, pp. 347–419, 2012.

[2] R. S. Harmon, R. E. Russo, and R. R. Hark, "Applications of laser-induced breakdown spectroscopy for geochemical and environmental analysis: A comprehensive review," *Spectrochimica Acta - Part B Atomic Spectroscopy*, vol. 87, pp. 11–26, 2013.

[3] A. A. Amosova, S. V. Panteeva, V. M. Chubarov, and A. L. Finkelshtein, "Determination of major elements by wavelength-dispersive X-ray fluorescence spectrometry and trace elements by inductively coupled plasma mass spectrometry in igneous rocks from the same fused sample (110 mg)," *Spectrochimica Acta - Part B Atomic Spectroscopy*, vol. 122, pp. 62–68, 2016.

[4] J. Savovic, M. Stoiljkovic, M. Kuzmanovic et al., "The feasibility of TEA CO2 laser-induced plasma for spectrochemical analysis of geological samples in simulated Martian conditions," *Spectrochimica Acta - Part B Atomic Spectroscopy*, vol. 118, pp. 127–136, 2016.

[5] J. M. Vadillo and J. J. Laserna, "Laser-induced breakdown spectroscopy of silicate, vanadate and sulfide rocks," *Talanta*, vol. 43, no. 7, pp. 1149–1154, 1996.

[6] F. Capitelli, F. Colao, M. R. Provenzano, R. Fantoni, G. Brunetti, and N. Senesi, "Determination of heavy metals in soils by Laser Induced Breakdown Spectroscopy," *Geoderma*, vol. 106, no. 1-2, pp. 45–62, 2002.

[7] R. Barbini, F. Colao, V. Lazic, R. Fantoni, A. Palucci, and M. Angelone, "On board LIBS analysis of marine sediments collected during the XVI Italian campaign in Antarctica," *Spectrochimica Acta-Part B Atomic Spectroscopy*, vol. 57, no. 7, pp. 1203–1218, 2002.

[8] B. Sallé, D. A. Cremers, S. Maurice, R. C. Wiens, and P. Fichet, "Evaluation of a compact spectrograph for in-situ and stand-off Laser-Induced Breakdown Spectroscopy analyses of geological samples on Mars missions," *Spectrochimica Acta - Part B Atomic Spectroscopy*, vol. 60, no. 6, pp. 805–815, 2005.

[9] B. Sallé, J.-L. Lacour, P. Mauchien, P. Fichet, S. Maurice, and G. Manhès, "Comparative study of different methodologies for quantitative rock analysis by Laser-Induced Breakdown Spectroscopy in a simulated Martian atmosphere," *Spectrochimica Acta - Part B Atomic Spectroscopy*, vol. 61, no. 3, pp. 301–313, 2006.

[10] N. Idris, K. Kagawa, F. Sakan, K. Tsuyuki, and S. Miura, "Analysis of heavy metal pollution in soil using transversely excited atmospheric CO2 laser-induced plasma by trapping the soil in microstructured holes on metal subtargets," *Applied Spectroscopy*, vol. 61, no. 12, pp. 1344–1351, 2007.

[11] J. M. Anzano, M. A. Villoria, A. Ruíz-Medina, and R. J. Lasheras, "Laser-induced breakdown spectroscopy for quantitative spectrochemical analysis of geological materials: Effects of the matrix and simultaneous determination," *Analytica Chimica Acta*, vol. 575, no. 2, pp. 230–235, 2006.

[12] M. Momcilovic, M. Kuzmanovic, D. Rankovic et al., "Optical emission studies of copper plasma induced using infrared transversely excited atmospheric (IR TEA) carbon dioxide laser pulses," *Applied Spectroscopy*, vol. 69, no. 4, pp. 419–429, 2015.

[13] A. Ruzicka, G. A. Snyder, and L. A. Taylor, "Comparative geochemistry of basalts from the moon, earth, HED asteroid, and mars: Implications for the origin of the moon," *Geochimica et Cosmochimica Acta*, vol. 65, no. 6, pp. 979–997, 2001.

[14] D. Campos, S. S. Harilal, and A. Hassanein, "The effect of laser wavelength on emission and particle dynamics of Sn plasma," *Journal of Applied Physics*, vol. 108, no. 11, p. 113305, 2010.

[15] G. W. Rieger, M. Taschuk, Y. Y. Tsui, and R. Fedosejevs, "Laser-induced breakdown spectroscopy for microanalysis using sub-millijoule UV laser pulses," *Applied Spectroscopy*, vol. 56, no. 6, pp. 689–698, 2002.

[16] V. Cvetković, D. Prelević, H. Downes, M. Jovanović, O. Vaselli, and Z. Pécskay, "Origin and geodynamic significance of Tertiary postcollisional basaltic magmatism in Serbia (central Balkan Peninsula)," *Lithos*, vol. 73, no. 3-4, pp. 161–186, 2004.

[17] M. Thompson and J. N. Walsh, *Handbook of inductively coupled plasma atomic emission spectrometry*, Viridian Publishing, Springer, Boston, MA, 1989.

[18] S. Zivkovic, J. Savovic, M. Trtica, J. Mutic, and M. Momcilovic, "Elemental analysis of aluminum alloys by Laser Induced Breakdown Spectroscopy based on TEA CO_2 laser," *Journal of Alloys and Compounds*, vol. 700, pp. 175–184, 2017.

[19] M. S. Trtica, B. M. Gaković, B. B. Radak, and Š. S. Miljanić, "An efficient small scale TEA CO2 laser for material surface modification," in *Proceedings of the International Conference on Atomic and Molecular Pulsed Lasers IV*, pp. 44–49, rus, September 2001.

[20] A. Khumaeni, M. Ramli, Y. Deguchi et al., "New technique for the direct analysis of food powders confined in a small hole using transversely excited atmospheric CO2 laser-induced gas plasma," *Applied Spectroscopy*, vol. 62, no. 12, pp. 1344–1348, 2008.

[21] A. Matsumoto, A. Tamura, K. Fukami, Y. H. Ogata, and T. Sakka, "Single-pulse underwater laser-induced breakdown spectroscopy with nongated detection scheme," *Analytical Chemistry*, vol. 85, no. 8, pp. 3807–3811, 2013.

[22] M. A. Khater, J. T. Costello, and E. T. Kennedy, "Optimization of the emission characteristics of laser-produced steel plasmas in the vacuum ultraviolet: significant improvements in carbon detection limits," *Applied Spectroscopy*, vol. 56, no. 8, pp. 970–983, 2002.

[23] S. Zivkovic, M. Momcilovic, A. Staicu, J. Mutic, M. Trtica, and J. Savovic, "Spectrochemical analysis of powdered biological samples using TEA CO_2 laser plasma excitation," *Spectrochimica Acta Part B: Atomic Spectroscopy*, vol. 128, pp. 22–29, 2017.

[24] R. B. Anderson, R. V. Morris, S. M. Clegg et al., "The influence of multivariate analysis methods and target grain size on the accuracy of remote quantitative chemical analysis of rocks using laser induced breakdown spectroscopy," *Icarus*, vol. 215, no. 2, pp. 608–627, 2011.

[25] R. Epstein, "Principles of Plasma Spectroscopy, by Hans R. Griem. Cambridge University Press, 1997, 366 pages. ISBN 0 521 45504 9. $100.00," *Journal of Plasma Physics*, vol. 60, no. 1, pp. 203–207.

[26] P. J. Linstrom and W. G. Mallard, "The NIST Chemistry WebBook: A chemical data resource on the Internet," *Journal of Chemical and Engineering Data*, vol. 46, no. 5, pp. 1059–1063, 2001.

[27] J. J. Olivero and R. L. Longbothum, "Empirical fits to the Voigt line width: A brief review," *Journal of Quantitative Spectroscopy and Radiative Transfer*, vol. 17, no. 2, pp. 233–236, 1977.

[28] M. Ivković and N. Konjević, "Stark width and shift for electron number density diagnostics of low temperature plasma: application to silicon laser induced breakdown spectroscopy," *Spectrochimica Acta Part B: Atomic Spectroscopy*, vol. 131, pp. 79–92, 2017.

[29] M. S. Dimitrijevic and S. Sahal-Brechot, "Stark Broadening of AI I Spectral Lines," *Physica Scripta*, vol. 49, no. 1, pp. 34–38, 1994.

[30] B. T. Fisher, H. A. Johnsen, S. G. Buckley, and D. W. Hahn, "Temporal gating for the optimization of laser-induced breakdown spectroscopy detection and analysis of toxic metals," *Applied Spectroscopy*, vol. 55, no. 10, pp. 1312–1319, 2001.